J|A|C|S
ARTICLES
Published on Web 03/11/2003

Synthesis of a Molecular $Mo_2Fe_6S_9$ Cluster with the Topology of the P^N Cluster of Nitrogenase by Rearrangement of an Edge-Bridged $Mo_2Fe_6S_8$ Double Cubane

Yugen Zhang and R. H. Holm*

Contribution from the Department of Chemistry and Chemical Biology, Harvard University, Cambridge, Massachusetts 02138

Received December 18, 2002; E-mail: holm@chemistry.harvard.edu

Abstract: The structures of the P cluster and cofactor cluster of nitrogenase are well-defined crystallographically. They have been obtained only by biosynthesis; their chemical synthesis remains a challenge. Synthetic routes are sought to the P cluster in the P^N state in which two cuboidal Fe_3S_3 units are connected by a μ_6-S atom and two Fe−(μ_2-S_{Cys})−Fe bridges. A reaction scheme affording a $Mo_2Fe_6S_9$ cluster in molecular form having the topology of the P^N cluster has been devised. Reaction of the single cubane $[(Tp)MoFe_3S_4Cl_3]^{1-}$ with PEt_3 gives $[(Tp)MoFe_3S_4(PEt_3)_3]^{1+}$ (**2**), which upon reduction with BH_4^- affords the edge-bridged all-ferrous double cubane $[(Tp)_2Mo_2Fe_6S_8(PEt_3)_4]$ (**4**) (Tp = tris(pyrazolylhydroborate(1−)). Treatment of **4** with 3 equiv of HS^- produces $[(Tp)_2Mo_2Fe_6S_9(SH)_2]^{3-}$ (**7**) as the Et_4N^+ salt in 86% yield. The structure of **7** is built of two $(Tp)MoFe_3(\mu_3\text{-}S)_3$ cuboidal fragments bridged by two μ_2-S atoms and one μ_6-S atom in an arrangement of idealized C_2 symmetry. The cluster undergoes three one-electron oxidation reactions and is oxidatively cleaved by *p*-tolylthiol to $[(Tp)MoFe_3S_4(S\text{-}p\text{-}tol)_3]^{2-}$ and by weak acids to $[(Tp)MoFe_3S_4(SH)_3]^{2-}$. The cluster core of **7** has the bridging pattern $[Mo_2Fe_6(\mu_2\text{-}S)_2(\mu_3\text{-}S)_6(\mu_6\text{-}S)]^{1+}$ with the probable charge distribution $[Mo^{3+}{}_2Fe^{2+}{}_5Fe^{3+}S_9]^{1+}$. Cluster **7** is a topological analogue of the P^N cluster but differs in having two heteroatoms and two Fe−(μ_2-S)−Fe instead of two Fe−(μ_2-S_{Cys})−Fe bridges. A best-fit superposition of the two cluster cores affords a weighted rms deviation in atom positions of 0.38 Å. Cluster **7** is the first *molecular* topological analogue of the P^N cluster. This structure had been prepared previously only as a fragment of complex high-nuclearity Mo−Fe−S clusters.

Introduction

We have recently emphasized the potential utility of high-nuclearity clusters whose metal and sulfide content exceed ca. six atoms each[1] as synthetic precursors to the cofactor cluster ($M_2Fe_6S_9$, M = Mo, V, Fe) and P cluster (Fe_8S_9) of nitrogenase.[2,3] The iron−molybdenum cofactor (FeMoco) and P cluster are well-described crystallographically in two oxidation states.[4,5] One such synthetic cluster type is the homo- or heterometallic edge-bridged double cubane whose $M_2Fe_6(\mu_3\text{-}S)_6(\mu_4\text{-}S)_2$ core structure is shown schematically in Figure 1. Examples with M = Fe,[6−8] V,[9] and Mo[10−14] have been prepared and are characterized by reduced (mainly Fe^{II}) oxidation levels and an $Fe_2(\mu_4\text{-}S)_2$ rhomb bridge unit. These clusters have actual or idealized centrosymmetry with heteroatoms M in transoid positions and contain the same number of metal atoms as and one sulfur atom less than both FeMoco and the P cluster. The latter is more relevant here. (Note that bridging cysteinate sulfur atoms are included in the core composition.) Its structure in the P^N (as-isolated) state, set out in Figure 1, is built of two distorted cubane units bridged by two μ_2-S_{Cys} and one μ_6-S atom with the bridging pattern $Fe_8(\mu_2\text{-}S)_2(\mu_3\text{-}S)_6(\mu_6\text{-}S)$. Until recently, no structure having the topology of the P^N cluster itself or as part of a larger structure had been prepared.

We have shown that the reaction of the double cubane $[(Cl_4cat)_2(Et_3P)_2Mo_2Fe_6S_8(PEt_3)_4]$[10,11] with $(Et_4N)(SH)$ under rather specific conditions affords the unprecedented cluster $[(Cl_4cat)_6(Et_3P)_6Mo_6Fe_{20}S_{30}]$,[8−] in which the iron atoms are present in tetrahedral FeS_4 sites with no terminal ligands and a mean oxidation state of ca. +2.4.[15] This cluster has a complex Fe−S bridging pattern. However, within it two $(Cl_4cat)_2(Et_3P)_2Mo_2Fe_6S_9$ fragments that structurally resemble the P^N cluster are readily discerned. (Abbreviations are defined in Chart 1.)

* Correspondence to this author.

(1) Zhou, H.-C.; Su, W.; Achim, C.; Rao, P. V.; Holm, R. H. *Inorg. Chem.* **2002**, *41*, 3191−3201.
(2) Howard, J. B.; Rees, D. C. *Chem. Rev.* **1996**, *96*, 2965−2982.
(3) Smith, B. E. *Adv. Inorg. Chem.* **1999**, *47*, 160−218.
(4) Peters, J. W.; Stowell, M. H. B.; Soltis, S. M.; Finnegan, M. G.; Johnson, M. K.; Rees, D. C. *Biochemistry* **1997**, *36*, 1181−1187.
(5) Mayer, S. M.; Lawson, D. M.; Gormal, C. A.; Roe, S. M.; Smith, B. E. *J. Mol. Biol.* **1999**, *292*, 871−891.
(6) Cai, L.; Segal, B. M.; Long, J. R.; Scott, M. J.; Holm, R. H. *J. Am. Chem. Soc.* **1995**, *117*, 8863−8864.
(7) Goh, C.; Segal, B. M.; Huang, J.; Long, J. R.; Holm, R. H. *J. Am. Chem. Soc.* **1996**, *118*, 11844−11853.
(8) Zhou, H.-C.; Holm, R. H. *Inorg. Chem.* **2003**, *42*, 0000.
(9) Hauser, C.; Bill, E.; Holm, R. H. *Inorg. Chem.* **2002**, *41*, 1615−1624.
(10) Demadis, K. D.; Campana, C. F.; Coucouvanis, D. *J. Am. Chem. Soc.* **1995**, *117*, 7832−7833.
(11) Osterloh, F.; Segal, B. M.; Achim, C.; Holm, R. H. *Inorg. Chem.* **2000**, *39*, 980−989.
(12) Osterloh, F.; Achim, C.; Holm, R. H. *Inorg. Chem.* **2001**, *40*, 224−232.
(13) Han, J.; Koutmos, M.; Al-Ahmad, S.; Coucouvanis, D. *Inorg. Chem.* **2001**, *40*, 5985−5999.
(14) Zhang, Y.; Zuo, J.-L.; Zhou, H.-C.; Holm, R. H. *J. Am. Chem. Soc.* **2002**, *124*, 14292−14293.
(15) Osterloh, F.; Sanakis, Y.; Staples, R. J.; Münck, E.; Holm, R. H. *Angew. Chem., Int. Ed.* **1999**, *38*, 2066−2070.

10.1021/ja0214633 CCC: $25.00

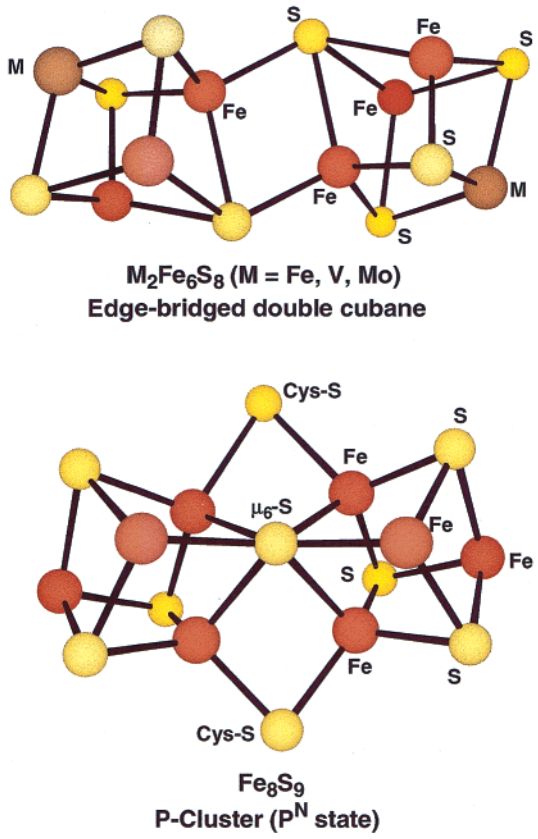

Figure 1. Schematic representations of the $M_2Fe_6S_9$ core (M = Fe, Mo, V) of homo- and heterometallic edge-bridged double cubanes (upper) and the Fe_8S_9 core of the P cluster of nitrogenase in the P^N state. In the edge-bridged cubanes, heteroatoms are always in transoid positions in idealized centrosymmetric structures. In the P^N cluster, bridging cysteinyl sulfur atoms are included in the core composition.

Thereafter, the cluster $[(Cl_4cat)_4(Et_3P)_4Mo_4Fe_{12}S_{20}K_3]^{5-}$ was prepared from a $[(Cl_4cat)(Et_3P)_2Mo_2Fe_6S_8(PEt_3)_4]/(Et_4N)(SH)$ reaction system conducted under different conditions than those that afforded the higher nuclearity cluster.[12] The structure of this cluster consists of two of the foregoing fragments bridged by two μ_2-S atoms and three K^+. The mean iron oxidation state is also close to +2.4. These results demonstrate that the P cluster topology is synthetically accessible, but as part of larger, more complex structures. Consequently, no clear synthetic pathway to $Mo_2Fe_6S_9$ clusters of the desired structure emerges from these synthetic reactions. Further, the properties of such clusters cannot be deconvoluted from those of the entire cluster. To redress this situation as part of our research on the synthesis of the clusters of nitrogenase, we have devised a route to the desired P-cluster structure in molecules with the core composition $M_2Fe_6S_9$ (M = Mo, V). Here we describe in detail the synthesis and certain properties of the molybdenum cluster. The synthesis is again based on an edge-bridged double cubane, but with a more symmetric coordination environment at the molybdenum atom. Corresponding results for the vanadium-containing cluster will be reported separately,[16] as will electronic properties of both clusters. This report expands our original description of $M_2Fe_6S_9$ clusters.[14]

Experimental Section

Preparation of Compounds. All operations were performed under a pure dinitrogen atmosphere using an inert atmosphere box or standard Schlenk techniques. Solvents were passed through an Innovative Technology solvent purification system prior to use.

$[(Tp)MoFe_3S_4(PEt_3)_3](BPh_4)$. To a solution of 110 mg (0.13 mmol) of $(Et_4N)[(Tp)MoFe_3S_4Cl_3]$[17] in 5 mL of acetonitrile was added 76 mg (0.65 mmol) of PEt_3. After 1 min, a solution of 260 mg (0.65 mmol) of $NaBPh_4$ in 1 mL of acetonitrile was introduced. The black reaction mixture was stirred for 12 h, and 20 mL of ether was added. The mixture was stirred for ca. 2 h and filtered through Celite to remove a white solid. The filtrate was reduced to dryness. The black residue was washed with ether and recrystallized from acetonitrile/ether to give the product as 120 mg (80%) of black platelike crystals. ^{1}H NMR (CD_3CN, cation): δ 3.3 (9), 7.4 (1), 13.2 (6), 13.7 (1), 17.3 (br, 1). $E_{1/2} = -0.79$ V (acetonitrile). This compound was identified by an X-ray structure determination.

$(Et_4N)_2[(Tp)MoFe_3S_4(SH)_3]$. A solution of 245 mg (0.20 mmol) of $[(Tp)MoFe_3S_4(PEt_3)_3](BPh_4)$ in 30 mL of acetonitrile was added to a solution of 110 mg (0.65 mmol) of $(Et_4N)(HS)$[18] in 10 mL of acetonitrile. The dark black solution was allowed to stand for 16 h and was filtered through Celite. Diffusion of ether into the filtrate caused the separation of black blocklike crystals. This material was recrystallized twice from acetonitrile/ether to yield the product as 105 mg (70%) of black crystals. ^{1}H NMR (CD_3CN, anion): δ 5.50 (1), 15.4 (1). $E_{1/2} = -0.89$ V (acetonitrile). Anal. Calcd for $C_{25}H_{53}BFe_3MoN_8S_7$: C, 31.14; H, 5.50; N, 11.63; Fe, 17.39; Mo, 9.96. Found: C, 31.14; H, 5.24; N, 12.21; Fe, 18.20; Mo, 10.34. A satisfactory S analysis was not obtained.

$[(Tp)_2Mo_2Fe_6S_8(PEt_3)_4]$. A solution of 250 mg (0.20 mmol) of $[(Tp)MoFe_3S_4(PEt_3)_3](BPh_4)$ in 5 mL of acetonitrile was added to a solution of 66 mg (0.26 mmol) of $(Bu_4N)(BH_4)$ in 1 mL of acetonitrile. The dark black solution was allowed to stand for 16 h, during which black platelike crystals separated. These were collected and washed with acetonitrile to afford the product as 117 mg (70%) of black crystalline solid. ^{1}H NMR (THF-d_8): δ 2.40 (18), 5.24 (2), 5.40 (1), 11.75 (12), 13.78 (2), 15.79 (1). $E_{1/2} = -0.72$ V (THF). Anal. Calcd for $C_{42}H_{60}B_2Fe_6Mo_2N_{12}P_4S_8$. C, 29.99; H, 4.79; N, 9.99; S, 15.25; Fe, 19.92; Mo, 11.41. Found: C, 30.10; H, 4.92; N, 10.08; S, 15.29; Fe, 19.89; Mo, 11.54.

$(Et_4N)_4[(Tp)_2Mo_2Fe_6S_8Cl_4]$. To a suspension of 160 mg (0.10 mmol) of $[(Tp)_2Mo_2Fe_6S_8(PEt_3)_4]$ in 15 mL of acetonitrile was added 66 mg (0.40 mmol) of Et_4NCl. A dark black solution formed within 1 h; it was stirred for 3 h and filtered through Celite. Diffusion of ether into the filtrate caused separation of a crystalline solid, which was collected and washed with ether to yield the product as 137 mg (73%) of black blocklike crystals. ^{1}H NMR (CD_3CN, anion): δ 5.4 (2), 13.9 (br, 1), 18.2 (v br), 19.0 (2) 26.4 (1). $E_{1/2} = -0.87$ V (acetonitrile). Anal. Calcd for $C_{50}H_{100}B_2Cl_4Fe_6Mo_2N_{16}S_8$: C, 32.04; H, 5.34; Fe, 17.80; Mo, 10.25; N, 11.96; S, 13.67. Found: C, 31.76; H, 5.30; Fe, 17.54; Mo, 10.28; N, 11.99; S, 13.81.

$(Et_4N)_2[(Tp)MoFe_3S_4(SCH_2Ph)_3]$. $[(Tp)_2Mo_2Fe_6S_8(PEt_3)_4]$ (101 mg, 0.060 mmol) was suspended in 10 mL of THF and treated with a solution of 67 mg (0.24 mmol) of $(PhCH_2S)_2S$ in 2 mL of THF. The dark brown suspension was stirred for 12 h and filtered through Celite. A suspension of 34 mg (0.24 mmol) of $(Et_4N)(BH_4)$ in 5 mL of THF was added to the filtrate. Slow diffusion of ether into the combined solution resulted in the separation of product as 105 mg (71%) of black platelike crystals. ^{1}H NMR (CD_3CN, anion): δ 5.8 (3), 5.9 (3), 7.5 (br), 8.5 (6), 14.7 (3), 70 (v br). This compound was identified by an X-ray structure determination.

$(Et_4N)_3[(Tp)_2Mo_2Fe_6S_9(SH)_2]\cdot 2MeCN$. Method A. $[(Tp)_2Mo_2Fe_6S_8(PEt_3)_4]$ (100 mg, 0.060 mmol) was suspended in 8 mL of acetonitrile, and a solution of 30 mg (0.18 mmol) of $(Et_4N)(HS)$ in 2 mL of acetonitrile was added, causing the solid to dissolve immediately. The

(16) Zuo, J.-L.; Zhou, H.-C.; Holm, R. H. Submitted for publication.
(17) Fomitchev, D. V.; McLauchlan, C. C.; Holm, R. H. *Inorg. Chem.* **2002**, *41*, 958−966.
(18) Heller, G.; Eysenbach, W. *Inorg. Chem.* **1979**, *18*, 380−383.

dark brown solution was stirred for 12 h and filtered through Celite. Slow diffusion of ether into the filtrate resulted in the separation of a solid, which was collected and dried to afford the product as 92 mg (86%) of a black crystalline solid. Absorption spectrum (acetonitrile): λ_{max} (ϵ_M) 335 (40 500), 570 (sh, 8000) nm. ^{1}H NMR (anion): δ 5.14 (2), 5.7 (br, 1), 8.30(1), 11.75 (2), 13.31 (1), 16.30 (2), 20. 93 (br, 1). $E_{1/2} = -0.43, -0.71, -1.09$ V (acetonitrile). Anal. Calcd for $C_{46}H_{88}B_2Fe_6Mo_2N_{17}S_{11}$: C, 31.02; H, 4.94; Fe, 18.81; Mo, 10.77; N, 13.36; S, 19.76. Found: C, 31.27; H, 4.88; Fe, 18.86; Mo, 10.74; N, 13.09; S, 19.88.

Method B. NaHS (120 mg, 0.22 mmol) was added to a solution of 94 mg (0.050 mmol) of $(Et_4N)_4[(Tp)_2Mo_2Fe_6S_8Cl_4]$ in 15 mL of acetonitrile. The reaction mixture was stirred for 12 h and filtered through Celite. Slow diffusion of ether into the filtrate resulted in formation of the product as 73 mg (82%) of black crystalline product, spectroscopically identical with the product of method A.

$(Et_4N)_2[(Tp)MoFe_3S_4(S\text{-}p\text{-}tol)_3]$. To a solution of 37 mg (0.020 mmol) of $(Et_4N)_3[(Tp)_2Mo_2Fe_6S_9(SH)_2]\cdot 2MeCN$ in 10 mL of acetonitrile was added a solution of 5.0 mg (0.044 mmol) of *p*-tolylthiol in 2 mL of acetonitrile. The dark brown solution was stirred for 12 h and filtered through Celite. Slow diffusion of ether into the filtrate resulted in the separation of a black powder and black platelike crystals. Mechanical separation, an X-ray structural analysis, and ^{1}H NMR established that the crystals contained the title compound. The powder has not been crystallized. With >6 equiv of thiol, the title compound was obtained as 36 mg (72%) after recrystallization from acetonitrile/ether. ^{1}H NMR (CD_3CN, anion): δ −3.20 (6) 5.90 (3), 13.9 (9), 14.8 (3),16.3 (6). The same compound, confirmed by X-ray analysis, was isolated in 26% yield from the reaction of the intial cluster with 4.4 equiv of NaS-*p*-tol in acetonitrile.

$(Et_4N)_5[(Tp)_4Mo_4Fe_{12}S_{14.5}Se_{5.5}]$. A suspension of 101 mg (0.060 mmol) of $[(Tp)_2Mo_2Fe_6S_8(PEt_3)_4]$ in 20 mL of acetonitrile was treated with a solution of 41 mg (0.20 mmol) of $(Et_4N)(HSe)$[19] in 2 mL of acetonitrile. The solid gradually dissolved, forming a dark brown solution, which was stirred for 12 h and filtered through Celite. Slow diffusion of ether caused separation of product as a black microcrystalline solid. This material was collected and washed with ether to give the product as 81 mg (77%) of a black microcrystalline solid. Absorption spectrum (acetonitrile): λ_{max} (ϵ_M) 335 (81 000) nm. ^{1}H NMR (anion): δ 5.3 (2), 5.7 (br), 7.8 (1),12.8 (2), 13.6 (1), 16.3 (2), 19.5 (1). Anal. Calcd for $C_{76}H_{140}B_4Fe_{12}Mo_4N_{29}S_{14.5}Se_{5.5}$: C, 26.38; H, 4.05; N, 11.82; Fe, 19.38; Mo, 11.09; S 13.42; Se, 12.56. Found: C, 26.34; H, 4.08; N, 11.75; Fe, 19.15; Mo, 10.30, S, 12.78; Se, 12.20.

In the sections that follow, clusters are numerically designated as **1**−**11** according to Chart 1.

Chart 1. Designation of Clusters[a] and Abbreviations[b]

$[(Tp)MoFe_3S_4Cl_3]^{1-}$	**1**[17]
$[(Tp)MoFe_3S_4(PEt_3)_3]^{1+}$	**2**
$[(Tp)MoFe_3S_4(SH)_3]^{2-}$	**3**
$[(Tp)_2Mo_2Fe_6S_8(PEt_3)_4]$	**4**
$[(Tp)_2Mo_2Fe_6S_8Cl_4]^{4-}$	**5**
$[(Tp)MoFe_3S_4(SCH_2Ph)_3]^{2-}$	**6**
$[(Tp)_2Mo_2Fe_6S_9(SH)_2]^{3-}$	**7**
$[(Tp)MoFe_3S_4(S\text{-}p\text{-}tol)_3]^{2-}$	**8**
$[(Tp)_4Mo_4Fe_{12}S_{14.5}Se_{5.5}]^{5-}$	**9**
$[(Cl_4cat)_6(Et_3P)_6Mo_6Fe_{20}S_{30}]^{8-}$	**10**[15]
$[(Cl_4cat)_4(Et_3P)_4Mo_4Fe_{12}S_{20}K_3(DMF)]^{5-}$	**11**[12]

[a] Here and elsewhere, ligands preceding the heterometal atom are bound to that atom. [b] Cl_4cat, tetrachlorocatecholate(2−); edt, 1,2-ethanethiolate-(2−); FeMoco, iron−molybdenum cofactor; tol, tolyl; Tp, tris(pyrazolyl)-hydroborate(1−).

X-ray Structure Determinations. The structures of the eight compounds listed in Tables 1 and 2 were determined. Suitable crystals of **[2]**(BPh_4), $(Et_4N)_4$**[5]**·2MeCN, $(Et_4N)_2$**[3**,**6**,**8]**, $(Et_4N)_3$**[7]**·9MeCN,

Table 1. Crystallographic Data for Compounds Containing Clusters **2**−**9**[a]

	[2](BPh_4)	$(Et_4N)_2$**[3]**	**[4]**	$(Et_4N)_4$**[5]**·2MeCN	$(Et_4N)_2$**[6]**	$(Et_4N)_3$**[7]**·9MeCN	$(Et_4N)_2$**[8]**	$(Et_4N)_5$**[9]**·8MeCN
formula	$C_{51}H_{75}B_2Fe_3Mo\text{-}N_6P_3S_4$	$C_{25}H_{53}B_1Fe_3Mo_1\text{-}N_8S_7$	$C_{21}H_{30}BFe_3Mo\text{-}N_6P_2S_4$	$C_{54}H_{106}B_2Cl_4Fe_6Mo_2\text{-}N_{18}S_8$	$C_{46}H_{71}B_1Fe_3Mo_1\text{-}N_8S_7$	$C_{60}H_{109}B_2Fe_6Mo_2\text{-}N_{24}S_{11}$	$C_{92}H_{142}B_2Fe_6Mo_2\text{-}N_{16}S_{14}$	$C_{92}H_{164}B_4Fe_{12}Mo_4\text{-}N_{37}S_{14}\ Se_6$
fw	1278.43	864.47	830.99	1954.44	1234.83	2067.97	2469.67	3808.34
cryst syst	rhombohedral	monoclinic	monoclinic	monoclinic	orthorhombic	monoclinic	monoclinic	orthorhombic
space group	$R\bar{3}$	$P2_1/n$	$P2_1/n$	$P2_1/n$	$Pca2_1$	$P2_1/n$	$P2_1/c$	$Aba2$
Z	6	4	4	4	4	4	4	4
a, Å	15.4332(8)	9.3437(9)	11.2863(9)	14.513(1)	18.155(5)	18.385(1)	34.136(8)	36.883(9)
b, Å	15.4332(8)	34.761(3)	25.282(2)	14.162(1)	16.731(4)	17.534(1)	11.871(3)	26.168(6)
c, Å	44.421(5)	12.005(1)	12.8320(9)	19.428(2)	18.149(5)	29.424(2)	31.277(7)	16.194(6)
α, deg	90	90	90	90	90	90	90	90
β, deg	90	91.266(2)	112.743(1)	94.503(2)	90	96.619(1)	116.927(4)	90
γ, deg	120	90	90	90	90	90	90	90
V, Å^3	9162.9(11)	3898.3(6)	3376.8(4)	3980.8(6)	5513(2)	9422.5(9)	11300(4)	15631(7)
GOF (F^2)	1.056	0.873	1.015	1.096	0.937	1.140	1.207	0.791
R_1,[b] wR_2[c]	0.066, 0.198	0.033, 0.067	0.049, 0.120	0.063, 0.124	0.049, 0.095	0.066, 0.151	0.12, 0.28	0.050, 0.100

[a] Collected using Mo Kα ($\lambda = 0.71073$ Å) radiation at $T = 213$ K. [b] $R_1 = \sum||F_o| - |F_c||/\sum|F_o|$. [c] $wR_2 = \{\sum[w(F_o^2 - F_c^2)^2]/\sum[w(F_o^2)^2]\}^{1/2}$.

(19) Krebs, B.; Bobb, W.; Wellmer, H.-J.; Wiesmann, K. *Z. Anorg. Allg. Chem.* **1994**, *620*, 1234−1246.

Table 2. Mean Values of Selected Bond Distances (Å) for Single Cubane Clusters **2**, **3**, **6**, and **8**

	Mo–N	Mo–S	Fe–S	Mo–Fe	Fe–Fe	Fe–P/S
$[TpMoFe_3S_4(PEt_3)_3]^+$ **2**	2.228(7)	2.369(2)	2.224(2)	2.670(1)	2.584(2)	2.309(3)
$[TpMoFe_3S_4(SH)_3]^{2-}$ **3**	2.240(3)	2.364(1)	2.277(1)	2.736(1)	2.710(1)	2.293(1)
$[(Tp)MoFe_3S_4(SCH_2Ph)_3]^{2-}$ **6**	2.239(5)	2.368(2)	2.279(2)	2.728(1)	2.710(1)	2.276(2)
$[(Tp)MoFe_3S_4(S\text{-}p\text{-}tol)_3]^{2-}$ **8**	2.24(2)	2.367(6)	2.276(7)	2.726(4)	2.693(6)	2.280(6)

and $(Et_4N)_5$[**9**]·8MeCN were obtained by ether diffusions into acetonitrile solutions; crystals of **4** were obtained from the preparative reaction. Crystals were mounted in Infineum oil and placed in a dinitrogen cold stream on a Siemens (Bruker) SMART CCD-based diffractometer. Cell parameters were retrieved using SMART software and refined using SAINT using all observed reflections. Data were collected at 0.3° intervals in ϕ and ω for 30 s/frame such that a hemisphere of data was collected. At total of 1271 frames were collected with a maximum resolution of 0.75 Å. The first 50 frames were recollected at the end of the data collection to monitor decay; none was found. The highly redundant data sets were reduced using SAINT and corrected for Lorentz and polarization effects. Absorption corrections were applied using SADABS supplied by Bruker. Structures were solved by direct methods using SHELXL-97. Metal atoms and first coordination sphere atoms were located from direct-methods *E*-maps; other non-hydrogen atoms were found in alternating difference Fourier syntheses and least-squares refinement cycles and, during final cycles, were refined anisotropically. Hydrogen atoms were placed in calculated positions and refined as riding atoms with a uniform value of U_{iso}. Crystallographic parameters and agreement factors are contained in Table 1.[20]

Other Physical Measurements. All measurements were performed under anaerobic conditions. ^{1}H NMR spectra were measured with a Varian AM-300 spectrometer. Cyclic voltammograms (100 mV/s) were recorded with a Princeton Applied Research Model 263 potentiostat/galvanostat using a Pt working electrode and 0.1 M $(Bu_4N)(PF_6)$ supporting electrolyte. Potentials are referenced to a SCE. Mössbauer spectra were collected with a constant acceleration spectrometer. Data were analyzed with WMOSS software (WEB Research Co., Edina, MN); isomer shifts are referenced to iron metal at room temperature.

Results and Discussion

In formulating synthetic routes to the clusters of nitrogenase, we utilize $MoFe_3S_4$ cubane-type clusters as intermediates to an $Mo_2Fe_6S_8$ edge-bridged double cubane. The latter is the immediate precursor to the octanuclear $Mo_2Fe_6S_9$ cluster that is of principal interest in this study. Single cubanes appear as reactants and products in the synthetic scheme of Figure 2. Because the structures of single cubanes[17,21,22] and edge-bridged double cubanes[10−12] have been presented and discussed at some length, a similar detailed presentation is not required here. The essential metric features of related species prepared in this work are summarized in Table 2 (**2**, **3**, **6**, **8**) and Figure 4 (**4**, **5**). Structures are provided in Figures 3−5. Clusters **1**−**9** were isolated as black crystalline salts (except neutral **4**), which are highly sensitive to dioxygen in the solid and in solution.

Synthesis Route and Structures of Intermediates. We seek individual molecular clusters, free of perturbing bridging interactions, approaching or achieving the topology of the P^N cluster. The current synthesis begins with trigonally symmetric **1**,[17] which has the $[MoFe_3S_4]^{3+}$ oxidation state usual for clusters of this type. In a precedented reaction type,[11] treatment with excess PEt_3 results in ligand substitution and core reduction to $[MoFe_3S_4]^{2+}$ with formation of [**2**](BPh_4) (80%). The structure of **2** (Figure 3) has a crystallographically imposed 3-fold axis and normal metric features (Table 2). The ^{1}H NMR spectrum, with Tp resonances at δ 7.4, 13.7, and 17.3 (br), is consistent with trigonal symmetry. The lability of the phosphine ligands is demonstrated by reaction 1 with 3 equiv of hydrosulfide and isolation of $(Et_4N)_2$[**3**], whose anion retains the cubane-type geometry (Figure 3). Cluster **2** is reversibly reduced electrochemically at $E_{1/2} = -0.79$ V in acetonitrile to the neutral cluster $[(Tp)MoFe_3S_4(PEt_3)_3]$ with the $[MoFe_3S_4]^{1+}$ oxidation level. When the reduction is performed chemically with borohydride, the product isolated is the edge-bridged double cubane **4** (70%). The ^{1}H NMR spectrum shows two types of pyrazolyl rings (δ 5.2, 13.8; 5.4, 15.8) in an intensity ratio of 2:1. Two of the 5-H resonances were not located, apparently because of paramagnetic broadening. Evidently, the phosphines are sufficiently labile to be displaced in the formation of the edge-bridged structure. The reaction is assisted by the very low solubility of **4** in acetonitrile. This cluster sustains facile ligand substitution, forming in reaction 2 chloride-ligated cluster **5** (73% as the Et_4N^+ salt), which maintains the edge-bridged structure.

$$[(Tp)MoFe_3S_4(PEt)_3]^{1+} + 3HS^- \rightarrow [(Tp)MoFe_3S_4(SH)_3]^{2-} + 3PEt_3 \quad (1)$$

$$[(Tp)_2Mo_2Fe_6S_8(PEt_3)_4] + 4Cl^- \rightarrow [(Tp)_2Mo_2Fe_6S_8Cl_4]^{4-} + 4PEt_3 \quad (2)$$

Clusters **4** and **5** are the only species known with the $[MoFe_3S_4]^{1+}$ oxidation level. Proof of the edge-bridged double cubane arrangement (Figure 1) follows from the X-ray determinations of the centrosymmetric structures in Figure 4. Their overall geometry closely resembles those of $[VFe_3S_4]^{1+}$ [9] and $[MoFe_3S_4]^{2+}$ [10,11,13] double cubanes reported previously. Several regularities emerge when the structures of **4** and **5** are compared with each other and with the double cubanes reported earlier. (i) Individual cubanes are linked through $Fe_2(\mu_4\text{-}S)_2$ rhombs with the angle at an iron atom larger than at a sulfur atom. In **4**, S4−Fe−S4′ = 108.4° and Fe1−S4−Fe1′ = 71.6°. (ii) The bridging Fe−(μ_4-S) bonds connecting individual cubanes are shorter than the other Fe−(μ_4-S) bonds and are marginally shorter than or about equal to the mean of Fe-μ_3S bonds within the cubanes. Again in **4**, Fe1−S4′ = 2.248(2) Å, Fe1−S4 = 2.455(1) Å, and Fe−(μ_3-S) = 2.267(1) Å (mean of 6). (iii) Fe−Fe separations in single and double cubanes with phosphine ligation are shorter than those in related clusters with terminal thiolate or halide ligands. The mean of three such distances in double cubanes **4** and **5** is 2.573(2) and 2.626(1) Å, respectively. Examples of this behavior in single cubanes are contained in

(20) See paragraph at the end of this article for Supporting Information available.
(21) Holm, R. H.; Simhon, E. D. Molybdenum/Tungsten−Iron−Sulfur Chemistry: Current Status and Relevance to the Native Cluster of Nitrogenase. In *Molybdenum Enzymes*; Spiro, T. G., Ed.; Wiley: New York, 1985; pp 1−87.
(22) Demadis, K. D.; Coucouvanis, D. *Inorg. Chem.* **1995**, *34*, 436−448.

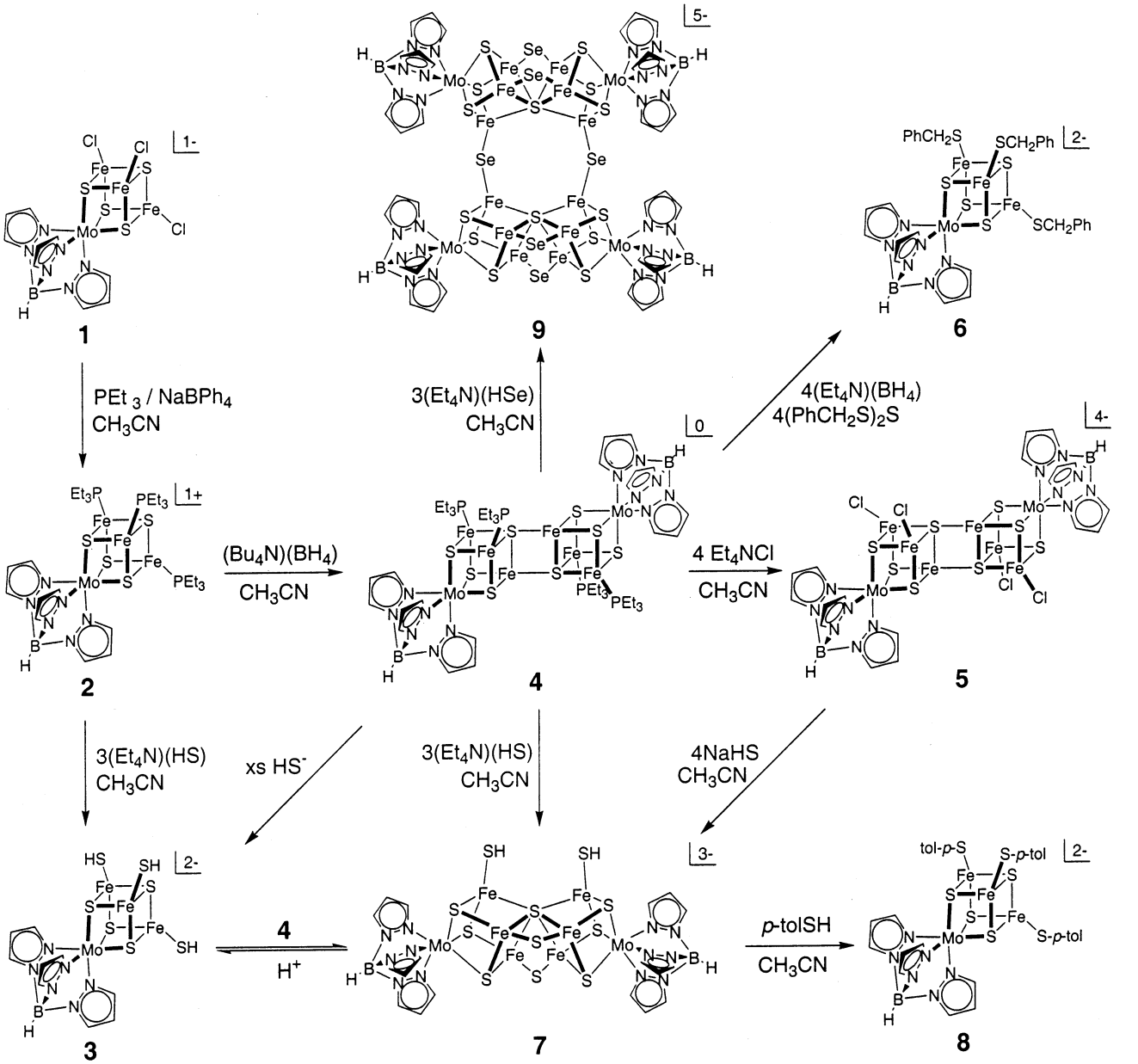

Figure 2. Synthetic scheme affording monocubane clusters **2**, **3**, **6**, and **8**, edge-bridged double cubanes **4** and **5**, cluster **7** with P cluster topology, and doubly bridged cluster **9** containing units with this topology.

Table 2 and may be found in prior work.[9,11,12,17] Numerical values given are typical for the entire set of double cubanes. Effect (i) is presumably driven largely by the tetrahedral stereochemical preference of four-coordinate high-spin Fe(II,III). Acute angles at sulfur in metal clusters are entirely common. The behavior in (ii) is opposite the usual bond length trend Fe-μ_2S < Fe-μ_3S < Fe-μ_4S displayed in clusters such as $[Fe_6S_9(SEt)_2]^{4-}$ [23] and $[(edt)_2Mo_2Fe_4S_9]^{4-}$ [1] Effect (iii) implies slightly enhanced Fe−Fe bonding in the presence of terminal phosphine ligands. At present, we cannot offer meaningful explanations of (ii) and (iii); these may require electronic structure calculations.

Oxidation States. Before proceeding with further reaction chemistry, attention is directed to the ^{57}Fe isomer shift data in Table 3. These data, withdrawn from a much larger set of results, illustrate two important points. (i) As the core oxidation level decreases at strict parity of terminal ligation, the isomer shifts δ and, consequently, the Fe(II) character of the core increase (**1** vs $[(Tp)MoFe_3S_4Cl_3]^{2-}$), there being usually a +(0.06−0.10) mm/s shift per electron added. (ii) Isomer shifts decrease in the order $\delta = Cl^- > RS^- > R_3P$ at parity of oxidation state[9] (**1** vs $[(Tp)MoFe_3S_4(SEt)_3]^{1-}$, **5** vs **4**). From previous arguments, the electron added to a $[MoFe_3S_4]^{3+,2+}$ core is essentially completely localized on the Fe_3S_4 fragment, leading to the $[Mo^{3+}Fe^{3+}Fe^{2+}{}_2] = [Mo^{3+}Fe^{2.33+}{}_3]$ formulation for the delocalized $[MoFe_3S_4]^{2+}$ core of three clusters of two single cubanes and one double cubane[11] in Table 3. Noting that the mean isomer shifts of $[(Cl_4\text{-cat})_2(Et_3P)_2Mo_2Fe_6S_8(PEt_3)_4]$ and **4** differ by 0.10 mm/s, we are led to the all-ferrous formulation $[Mo^{3+}Fe^{2+}{}_3]$ for the $[MoFe_3S_4]^{1+}$ cores of **4** and isoelectronic **5**. Clusters **4** and **5** are oxidized at −0.72 V in THF and −0.87 V in acetonitrile, respectively. Neither shows a reversible reduction step, consistent with an

(23) Hagen, K. S.; Watson, A. D.; Holm, R. H. *J. Am. Chem. Soc.* **1983**, *105*, 3905−3913.

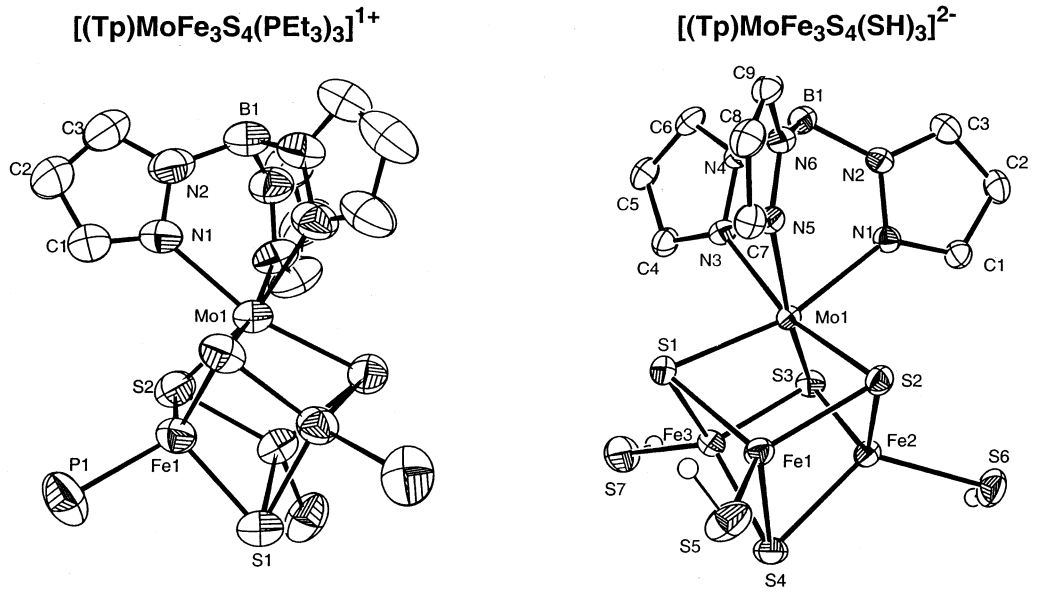

Figure 3. Structures of $[(Tp)MoFe_3S_4(PEt_3)_3]^{1+}$ (left) and $[(Tp)MoFe_3S_4(SH)_3]^{2-}$ (right) showing 50% probability ellipsoids and atom-numbering schemes. $[(Tp)MoFe_3S_4(PEt_3)_3]^{1+}$ has a crystallographically imposed C_3 axis. In $[(Tp)MoFe_3S_4(SH)_3]^{2-}$, the hydrosulfide hydrogen atoms were located and refined.

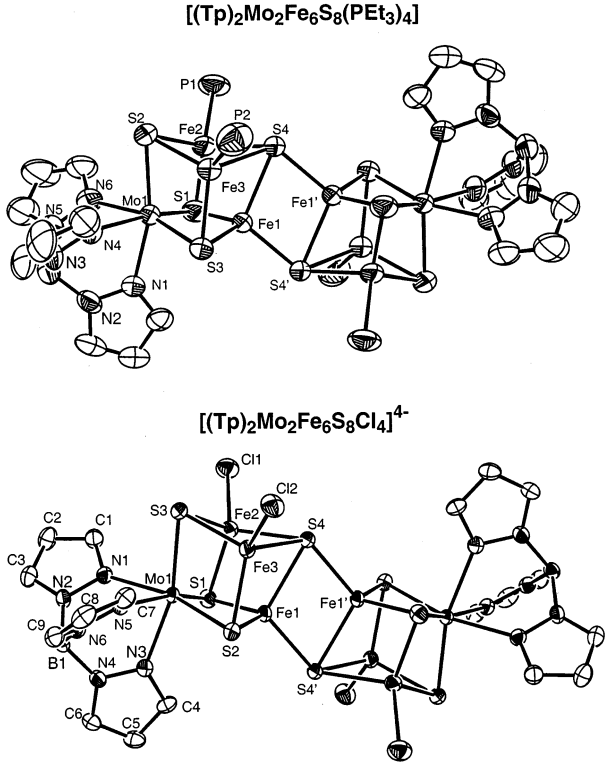

Figure 4. Structures of the edge-bridged double cubanes $[(Tp)_2Mo_2Fe_6S_8(PEt_3)_4]$ (upper) and $[(Tp)_2Mo_2Fe_6S_8Cl_4]^{4-}$ (lower) showing 50% probability ellipsoids and atom-numbering schemes. Primed and unprimed atoms are related by crystallographically imposed centrosymmetry. Selected mean bond distances (Å) and angles (deg) for $[(Tp)_2Mo_2Fe_6S_8(PEt_3)_4]$: Mo−N, 2.247(7); Mo−S, 2.383(2); Mo−Fe, 2.684(1); Fe−Fe, 2.573(2) (mean of 3); Fe−S, 2.267(3) (mean of 6 for S1, S2, S3); Fe1−S4, 2.455(2); Fe2−S4, 2.366(3); Fe3−S4, 2.373(3); Fe1−S4′, 2.248(2); Fe1−Fe1′, 2.757(2); Fe1−S4−Fe1′, 71.62(7); S4−Fe1−S4′, 108.38(7). For $[(Tp)_2Mo_2Fe_6S_8Cl_4]^{4-}$: Mo−N, 2.246(4); Mo−S, 2.384(1); Mo−Fe, 2.737(1); Fe−Fe, 2.626(1) (mean of 3); Fe−S, 2.286(1) (mean of 6 for S1, S2, S3); Fe1−S4, 2.426(1); Fe2−S4, 2.401(1); Fe3−S4, 2.373(1); Fe1−S4′, 2.283(1); Fe1−Fe1′, 2.737(1); Fe1−S4−Fe1′, 70.73(4); S4−Fe1−S4′, 109.1(4).

all-ferrous description. Double cubane **4** is the first all-ferrous $MoFe_3S_4$ cluster whose reactivity has been investigated.

Reactions of $[(Tp)_2Mo_2Fe_6S_8(PEt_3)_4]$ with $S^{0,2-}$ Reagents. Edge-bridged double cubanes have proven to be useful, and possibly, unique, precursors to other high-nuclearity clusters.[13,24] In our hands, they have afforded the complicated species **10**[15] and, subsequently, **11**,[12] which contain fragments with the topology of the P^N cluster (Figure 1). In this work, we have sought a route to this fragment in molecular form. To increase the sulfur content of the cluster core, two reagents have been investigated.

In an attempt to increase the core stoichiometry to $Mo_2Fe_6S_9$ with concomitant core oxidation, the reaction of **4** with benzyl trisulfide in acetonitrile was investigated. However, only an intractable black solid was obtained. Addition of a reducing agent (to promote formation of sulfide) and further variation of conditions led finally to the formation of the benzylthiolate-ligated single cubane **6**, isolated as the Et_4N^+ salt (71%). The product contains an oxidized ($[MoFe_3S_4]^{2+}$) core and was identified by the X-ray structure in Figure 5; the cluster is isodimensional with **3** (Table 2). Its formation proceeds by the apparent stoichiometry of reaction 3. Because a single cubane is not the desired product, further experiments involved the use of reduced sulfur as hydrosulfide.

$$[(Tp)_2Mo_2Fe_6S_8(PEt_3)_4] + 4(PhCH_2S)_2S + 4BH_4^- \rightarrow 2[(Tp)MoFe_3S_4(SCH_2Ph)_3]^{2-} + 4Et_3PS + PhCH_2SSCH_2Ph + 4BH_3 + 2H_2 \quad (3)$$

Treatment of **4** with 3 equiv of hydrosulfide in acetonitrile results in the formation of the new cluster **7**, isolated as black crystalline $(Et_4N)_3$[**7**]·2MeCN (86%). Product formation is interpreted in terms of reaction 4. (In our earlier report,[14] we used 4 equiv of hydrosulfide, but have subsequently found that only 3 equiv is necessary for a high yield conversion of **4** to **7**.) One-half equivalent of dihydrogen is included to account for the core oxidation level $[Mo_2Fe_6S_9]^{1+}$, one electron more

(24) Coucouvanis, D.; Han, J.; Moon, N. *J. Am. Chem. Soc.* **2002**, *124*, 216−224.

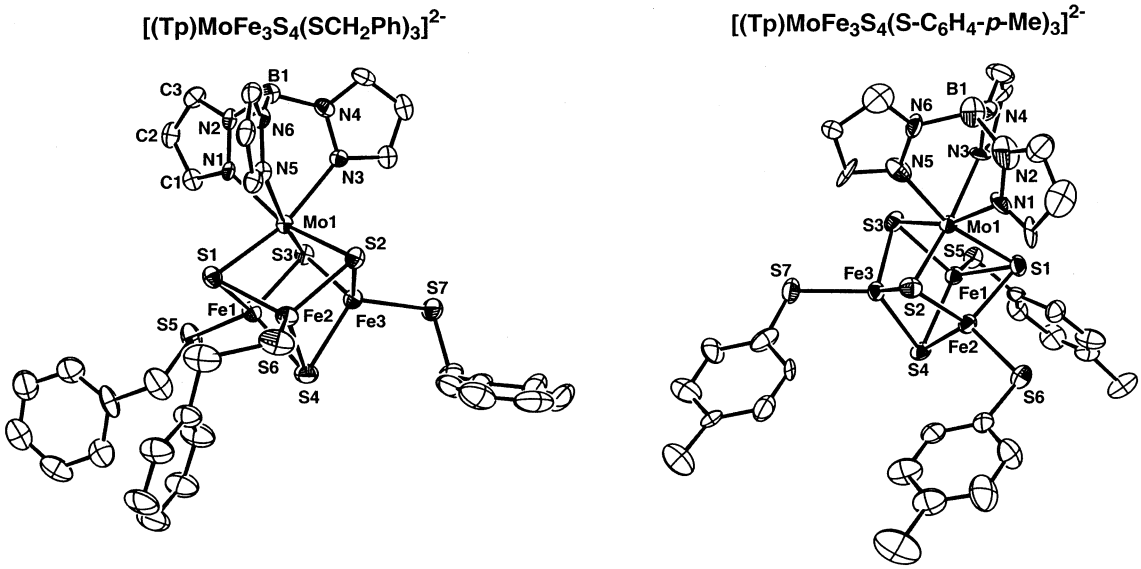

Figure 5. Structures of $[(Tp)MoFe_3S_4(SCH_2Ph)_3]^{2-}$ (left) and $[(Tp)MoFe_3S_4(S\text{-}p\text{-}tol)_3]^{2-}$ (right) showing 50% probability ellipsoids and atom-numbering schemes.

Table 3. Zero-Field Mössbauer Parameters of $MoFe_3S_4$ Clusters[a]

cluster	δ (mm/s)[b]	ΔE_Q (mm/s)[b]	ref
$[(Tp)MoFe_3S_4Cl_3]^{1-}$ (**1**)	0.51(2), 0.46(1)	1.09(2), 0,0.61(1)	17
$[(Tp)MoFe_3S_4(SEt)_3]^{1-}$	0.39	1.02	17
$[(Tp)MoFe_3S_4Cl_3]^{2-}$	0.62 (2), 0.59(2)	1.15(2), 0.62(1)	17
$[(Cl_4cat)(MeCN)MoFe_3S_4(PBu^t_3)_3]$	0.53(2), 0.51(1)	0.75(2), 2.27(1)	11
$[(Cl_4cat)_2(Et_3P)_2Mo_2Fe_6S_8(PEt_3)_4]$	0.48(7), 0.45(3)	0.72(7), 2.30(3)	12
$[(Tp)_2Mo_2Fe_6S_8(PEt_3)_4]$ (**4**)	0.56(2), 0.58(1)	1.05(2), 0.54(1)	*c*
$[(Tp)_2Mo_2Fe_6S_8Cl_4]^{4-}$ (**5**)	0.74(2), 0.64(1)	0.92(2), 0.67(1)	*c*
$[(Tp)_2Mo_2Fe_6S_9(SH)_2]^{3-}$ [e] (**7**)	0.55	0.62[e]	*c*
$[(Cl_4cat)_6(Et_3P)_6Mo_6Fe_{20}S_{30}]^{8-}$ [d,e] (**10**)	0.47	0.8[e]	15
$[(Cl_4cat)_4(Et_3P)_4Mo_4Fe_{12}S_{20}K_3(DMF)]^{5-}$ (**11**)	0.51	0.82	12

[a] Data at 4.2 K unless otherwise indicated. [b] Relative intensities of quadrupole doublets in parentheses. [c] This work. [d] 150 K. [e] Broadened quadrupole doublet.

oxidized than $2[MoFe_3S_4]^{1+} + S^{2-}$; the oxidant has not been directly identified.

$$[(Tp)_2Mo_2Fe_6S_8(PEt_3)_4] + 3HS^- \rightarrow [(Tp)_2Mo_2Fe_6S_9(SH)_2]^{3-} + 4PEt_3 + 1/2H_2 \quad (4)$$

Other synthetic methods for **7** were investigated. Double cubane **5** with 4 equiv of NaHS in acetonitrile affords the cluster in 82% yield as the Et_4N^+ salt. When equimolar amounts of **3** and **4** were allowed to react in acetonitrile for 16 h, **7** was observed as the major product by ^{1}H NMR (vide infra). Neither of these reactions has an advantage over reaction 4, which in multiple runs has proven to be highly reproducible.

$[(Tp)_2Mo_2Fe_6S_9(SH)_2]^{3-}$. (a) Structure. The structure of cluster **7** is shown in two perspectives in Figure 6; selected bond angles and distances are collected in Table 4. Reaction 4 proceeds with displacement of the phosphine ligands, substantial core rearrangement with incorporation of one additional sulfide atom, and binding of two terminal hydrosulfide ligands. Comparison with Figure 1 immediately reveals that **7** adopts the P^N cluster topology, consisting of two $MoFe_3(\mu_3\text{-}S)_3$ cuboidal fragments linked by two μ_2-S atoms simulating two μ_2-S_{Cys} bridges and one μ_6-S atom. The core bridging pattern is $[Mo_2Fe_6(\mu_2\text{-}S)_2(\mu_3\text{-}S)_6(\mu_6\text{-}S)]^{1+}$. Each iron atom has distorted tetrahedral FeS_4 coordination. The cluster has idealized C_2 symmetry. The overall structure is usefully described with reference to two core least-squares planes. Atom deviations from the plane Mo(1,2)Fe(2,3,5,6) are ≤0.050 Å. At the center of the plane is the slightly irregular rectangle Fe(2,3,5,6) with two distances Fe2−Fe5 = 2.697(2) Å and Fe3−Fe6 = 2.718(2) Å, two longer distances Fe2−Fe3 = 2.750(1) Å and Fe5−Fe6 = 2.764(1) Å, and Fe−Fe−Fe angles of 89.6−90.8°. Atoms Fe1 and Fe4 lie on the same side of the plane at displacements of 2.209 and 2.223 Å, respectively. The atoms μ_3-S(1,3,4,6) are on this side at 1.254−1.366 Å, as is μ_6-S(8) at 1.430 Å. The atoms μ_3-S(2,5) are located on this opposite site at 1.653−1.665 Å, as are μ_2-S(7,9) but at the much smaller displacements of 0.500−0.594 Å. Atom deviations from the plane Mo(1,2)Fe(1,4)S(2,5,8) are ≤0.061 Å. This plane forms a dihedral angle of 90° with the first plane. Hydrosulfide ligands S10 (0.243 Å) and S11 (0.331 Å) lie on opposite sides of this plane with the indicated displacements.

Fragments of the initial cluster **4** are evident as two (Tp)$MoFe_3S_3$ portions of **7** (e.g., Mo(1)Fe(1−3)S(1−3)) within which dimensional changes are small. The molybdenum atoms retain distorted octahedral coordination, and mean Mo−N, Mo−S, and Mo−Fe distances change by ≤0.04 Å. The major structural changes in the **4** → **7** conversion are the deconstruction of the bridging rhomb, formation of two bridges centered at μ_2-S(7,9), and creation of six bridges centered at μ_6-S8 between

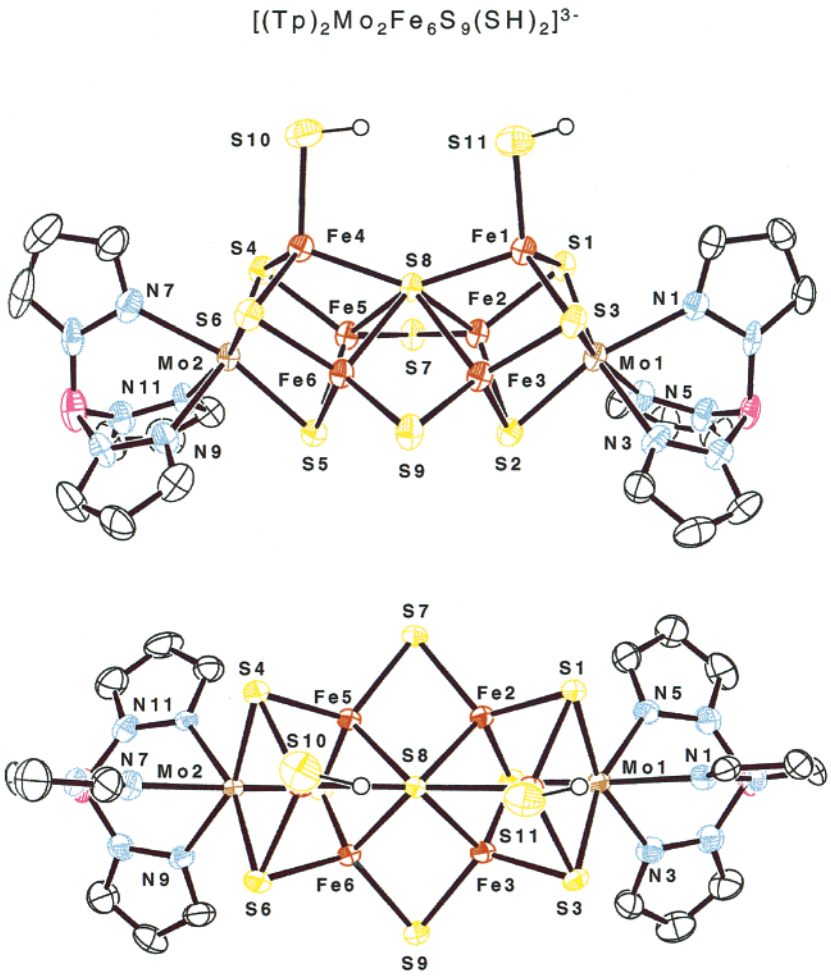

Figure 6. Structure of $[(Tp)_2Mo_2Fe_6S_9(SH)_2]^{3-}$ displayed using a side view (upper) and top view (lower) and showing 50% probability ellipsoids and atom-numbering schemes.

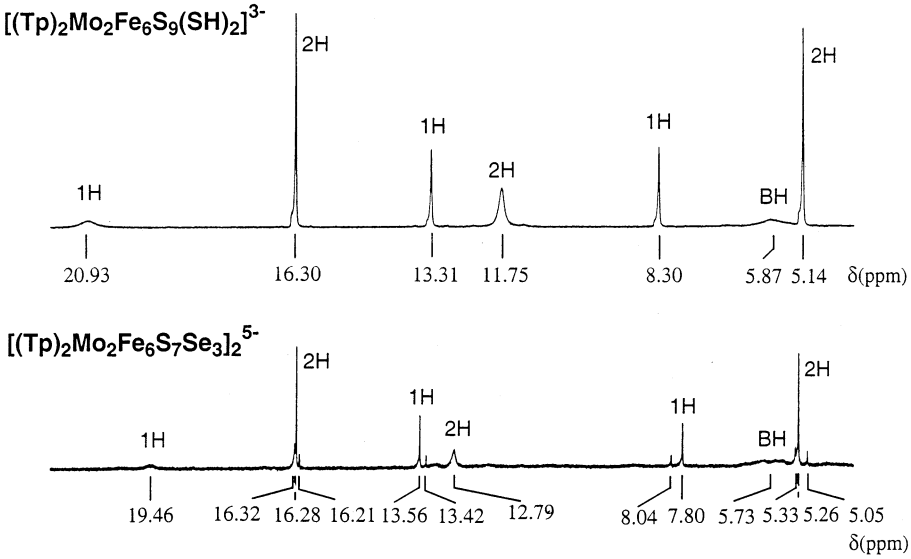

Figure 7. ^1H NMR spectra of $[(Tp)_2Mo_2Fe_6S_9(SH)_2]^{3-}$ and $[(Tp)_2Mo_2Fe_6S_7Se_3]_2^{5-}$ in CD_3CN solutions at ambient temperature. The 2:1 ratio of inequivalent pyrazolyl rings is indicated by the relative signal intensities.

the Fe_3 faces of two cuboidal fragments. Dimensions of the μ_2-bridges are normal, mean values of Fe−S−Fe angles and Fe−S distances being 75.0(3)° and 2.224(5) Å, respectively. Other bond distances are not exceptional, and Fe−S bond lengths, unlike those of **4**, adhere to the order Fe-μ_2S > Fe-μ_3S > Fe-μ_4S. For example, note the distances Fe3−(μ_2-S9) = 2.232(3) Å, Fe3−(μ_3-S2) = 2.266(3) Å, and Fe3−(μ_6-S8) = 2.398(2) Å.

The sextuple bridging atom S8 and its associated interactions comprise the most exceptional part of the structure of **7**. At

Table 4. Selected Bond Distances (Å) and Angles (deg) for $[(Tp)_2Mo_2Fe_6S_9(SH)_2]^{3-}$

Mo1−N1	2.259(8)	Mo2−N7	2.232(7)
Mo1−N3	2.240(7)	Mo2−N9	2.249(8)
Mo1−N5	2.238(7)	Mo2−N11	2.251(8)
Mo1−S1	2.377(2)	Mo2−S4	2.370(2)
Mo1−S2	2.358(3)	Mo2−S5	2.356(2)
Mo1−S3	2.376(2)	Mo2−S6	2.393(2)
Mo1−Fe1	2.697(1)	Mo2−Fe4	2.707(1)
Mo1−Fe2	2.726(1)	Mo2−Fe5	2.731(1)
Mo1−Fe3	2.741(1)	Mo2−Fe6	2.724(1)
Fe1−S1	2.264(3)	Fe4−S4	2.262(3)
Fe1−S3	2.253(3)	Fe4−S6	2.275(3)
Fe1−S8	2.391(2)	Fe4−S8	2.357(2)
Fe1−S10	2.280(3)	Fe4−S11	2.295(3)
Fe2−S1	2.260(3)	Fe5−S4	2.251(3)
Fe2−S2	2.270(3)	Fe5−S5	2.271(3)
Fe2−S7	2.221(3)	Fe5−S7	2.225(3)
Fe2−S8	2.391(2)	Fe5−S8	2.396(3)
Fe3−S2	2.266(3)	Fe6−S5	2.255(3)
Fe3−S3	2.261(3)	Fe6−S6	2.265(3)
Fe3−S8	2.398(2)	Fe6−S8	2.383(3)
Fe3−S9	2.232(3)	Fe6−S9	2.220(3)
Fe1−Fe2	2.739(2)	Fe4−Fe5	2.724(2)
Fe1−Fe3	2.726(2)	Fe4−Fe6	2.756(2)
Fe2−Fe3	2.750(2)	Fe5−Fe6	2.764(2)
Fe2−Fe5	2.697(2)	Fe3−Fe6	2.718(2)
Fe1−Fe4	4.444(3)		
Fe2−S7−Fe5	74.69(8)	Fe3−S9−Fe6	75.24(9)
Fe4−S8−Fe5	69.93(7)	Fe1−S8−Fe3	69.91(7)
Fe4−S8−Fe6	71.10(7)	Fe1−S8−Fe2	70.41(7)
Fe2−S8−Fe3	70.08(7)	Fe5−S8−Fe6	70.66(7)
Fe2−S8−Fe5	68.57(7)	Fe3−S8−Fe6	69.28(7)
Fe2−S8−Fe6	109.1(1)	Fe3−S8−Fe5	106.3(1)
Fe1−S8−Fe5	137.2(1)	Fe2−S8−Fe4	135.3(1)
Fe1−S8−Fe6	136.2(1)	Fe3−S8−Fe4	138.8(1)
Fe1−S8−Fe4	141.0(1)		

atom μ_6-S8 there are 15 independent Fe−S−Fe angles, which under idealized C_2 symmetry reduce to seven equivalent pairs and one unique angle.[25] Members of an equivalent pair are located on the same line in Table 4. Four pairs, exemplified by Fe1−S8−Fe3, Fe1−S8−Fe2, Fe2−S8−Fe3, and Fe2−S8−Fe5, measure the acute angles at S8 and cover the range 68.6−71.1° with a mean of 70.0(8)°. Another pair, Fe2−S8−Fe6 (109.1°) and Fe3−S8−Fe5 (106.3°), describes the triangular faces in the central Fe_4S pyramid. Two other pairs, represented by Fe1−S8−Fe6 and Fe2−S8−Fe5, are at 135.3−138.8° with a mean of 137(1)° and delimit angles involving Fe(1,4) and Fe(2,3,5,6) of the interior rectangle. The angle Fe1−S8−Fe4 = 141.0(1)° is unique and is the largest Fe−S−Fe bonded angle in the structure. Comparison of the core of **7** with the $Mo_2Fe_6S_9$ fragments of **10**[15] and **11**[12] leave no doubt that the former is an isostructural molecular version of these fragments. The angle analogous to Fe1−S8−Fe4 is 135.3(2)° in **10** and 138.9(7)° in **11.** A best-fit superposition of the $Mo_2Fe_6S_9$ core of **7** with the Fe_8S_9 core of the P^N cluster[5] affords a weighted rms deviation in atom positions of 0.38 Å. The corresponding value for the $Fe_6(\mu_6$-S) portion is 0.24 Å.[26] The differences of an Mo_2Fe_6 instead of an Fe_8 metal content and two μ_2-S instead of two μ_2-S_{Cys} bridges notwithstanding, we conclude that cluster **7** and its vanadium analogue $[(Tp)_2V_2Fe_6S_9(SH)_2]^{4-}$ [14] are the initial examples of molecular topological analogues of the P^N cluster of nitrogenase.

(25) The number of independent Fe−(μ_6-S)−Fe angles is eight, not nine as previously stated.[14]
(26) For an example of a best-fit superposition, cf. Figure 9 of ref 12.

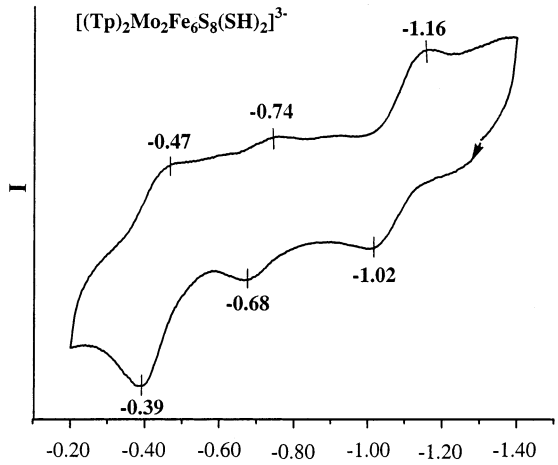

Figure 8. Cyclic voltammogram (100 mV/s) of $[(Tp)_2Mo_2Fe_6S_9(SH)_2]^{3-}$ in acetonitrile solution at ambient temperature. Peak potentials are indicated.

(b) Selected Properties. With the structure of **7** clarified, the advantage of a trigonally symmetric terminal ligand at the molybdenum sites becomes apparent. This ligand serves two purposes. It acts as a protecting group, directing reactions to the more labile iron sites. In the construction of sulfide-bridged double cubanes, we had employed *N*-methylimidodiacetate(2−) for a similar purpose.[27,28] Tridentate ligands L−L′−L at heterometal sites can potentially generate two diastereomers with the P^N cluster topology. A trigonally symmetric ligand does not lead to isomers, a matter that may contribute to the high crystallinity of the isolated salt of **7**. In acetonitrile solution, cluster **7** exhibits the ^{1}H NMR spectrum shown in Figure 7, containing two sets of pyrazolyl proton signals in an intensity ratio of 2:1, consistent with the solid state structure. The Mössbauer spectrum of **7** consists of a broadened quadrupole doublet. The isomer shift $\delta = 0.55$ mm/s (4.2 K, Table 3) shows that the cluster is substantially reduced and presumably describable as $[Mo^{3+}{}_2Fe^{2+}{}_5Fe^{3+}S_9]^{1+}$, although this formulation cannot be demonstrated from the isomer shift alone. However, one implication is that **7** should be susceptible to oxidation. Indeed, **7** shows three oxidation steps at $E_{1/2} = -1.09$, -0.71, and -0.43 V in the cyclic voltammogram of Figure 8.

In an attempt to substitute the hydrosulfide ligands, **7** was treated with 2 equiv of either of the weak acids pyridinium triflate or $(Et_3NH)(BPh_4)$ in acetonitrile. Black platelike crystals of $(Et_4N)_2$[**3**], identified crystallographically, were obtained in ca. 20% yield. Given this relationship between **3** and **7** and electrochemical detection of a 2− cluster derived from **7**, the conceivable reaction $2[(Tp)MoFe_3S_4(SH)_3]^{2-} \rightarrow [(Tp)_2Mo_2Fe_6S_9(SH)_2]^{2-} + 2HS^- + H_2S$ was investigated. However, no tractable cluster product was obtained. In a further experiment, **7** was reacted with 2 equiv of *p*-tolylthiol in acetonitrile. A small quantity of black crystals was obtained and shown by an X-ray crystal structure to be $(Et_4N)_2$[**8**], whose anion has a single cubane structure (Figure 5). The cluster is isometric with **3** and **6** (Table 2). Reaction of **7** with >6 equiv of the thiol afforded the product compound in 72% yield. In the formation of **3** and **8** from **7**, the observed oxidative conversion is $[Mo_2Fe_6S_9]^{1+} \rightarrow 2[MoFe_3S_4]^{2+} + S^{2-} + e^-$. It is interpreted in terms of

(27) Huang, J.; Mukerjee, S.; Segal, B. M.; Akashi, H.; Zhou, J.; Holm, R. H. *J. Am. Chem. Soc.* **1997**, *119*, 8662−8674.
(28) Huang, J.; Holm, R. H. *Inorg. Chem.* **1998**, *37*, 2247−2254.

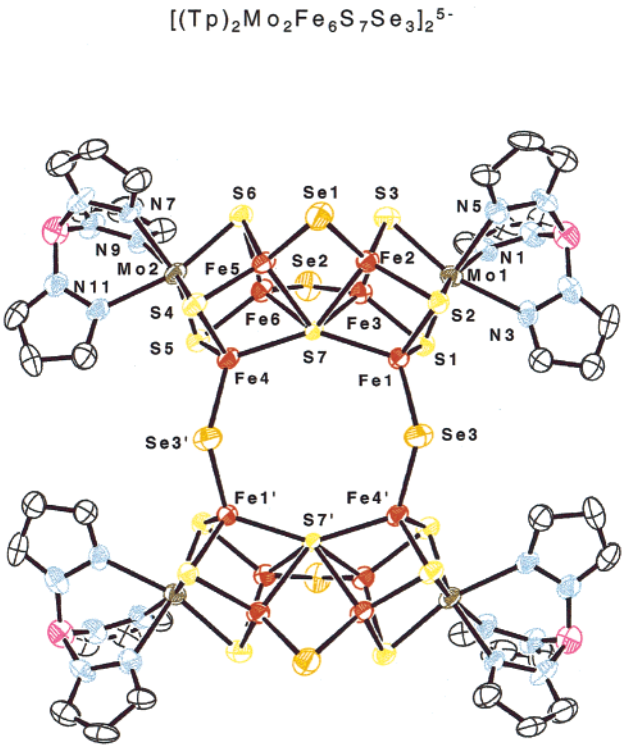

Figure 9. Structure of $[(Tp)_2Mo_2Fe_6S_7Se_3]_2^{5-}$ showing 50% probability ellipsoids and the atom-numbering scheme. Primed and unprimed atoms are related by a crystallographically imposed C_2 axis.

reaction 5 (R = *p*-tol, H), in which dihydrogen is invoked as a reduced product.

$$[(Tp)_2Mo_2Fe_6S_9(SH)_2]^{3-} + 6RSH \rightarrow 2[(Tp)MoFe_3S_4(SR)_3]^{2-} + 3H_2S + H^+ + {}^1/_2H_2 \quad (5)$$

(c) Selenide Substitution. We have sought to address one question about the obviously complicated pathway of reaction 4; namely, what is the fate of the externally added sulfide in the structure of product cluster **7**? Because it is well established that cubane-type Fe−S/Se[29,30] and M−Fe−S/Se[31] clusters are isostructural (but not isodimensional), the same outcome can be expected for any selenide variant of **7**. Consequently, 3.3 equiv of HSe^- was employed in place of HS^- in reaction 4. The product isolated fit the analytical composition $(Et_4N)_5[(Tp)_4Mo_4Fe_{12}S_{14.5}Se_{5.5}]$ with the experimental atom ratio S/Se = 2.58:1. The structure of product cluster **9**, set out in Figure 9, consists of two fragments $[(Tp)_2Mo_2Fe_6Q_9]^{0,1-}$ doubly bridged by μ_2-Q(3,3′) (Q = S, Se) and related by a C_2 axis. The bridge atoms occupy the positions of the hydrosulfide ligands in **7**. The cluster contains the $[Mo_2Fe_6Q_9]^{1+}$ and $[Mo_2Fe_6Q_9]^{2+}$ cores, which are one and two electrons more oxidized, respectively, than $[Mo_2Fe_6S_8]^{2+} + Se^{2-}$. The 1+ core is present in **7** and the 2+ core is its first oxidation product, detected electrochemically. The formation of **9** is rationalized by reaction 6, in which the simplifying assumptions that 3 equiv of H^+ are reduced and that H_2S and not H_2Se is formed. We cannot account for the formation of the bridged double−double cubane structure and could not predict the formation of mixed core oxidation states. Evidently, the putative core oxidation state $[Mo_2Fe_6Q_9]^0$ is a strong reductant. We do note, however, that the doubly bridged architecture of **9** is also found in **11**, where potassium ions also occupy bridging positions.[12]

Table 5. Selected Bond Distances (Å) and Angles (deg) for $[(Tp)_2Mo_2Fe_6S_7Se_3]_2^{5-}$

Mo−N	2.243(8)	Mo−S	2.365(3)
Mo−Fe	2.712(2)	Fe−(μ_3-S)[a]	2.248(3)
Fe−Fe[a]	2.761(2)	Fe2−Fe5	2.722(2)
Fe3−Fe6	2.681(2)	Fe1−S7	2.370(2)
Fe1−Se3	2.303(2)	Fe2−S7	2.436(2)
Fe2−Se1	2.340(2)	Fe3−S7	2.439(3)
Fe3−Se2	2.324(2)	Fe4−S7	2.385(2)
Fe4−Se3′	2.312(2)	Fe5−S7	2.420(2)
Fe5−Se1	2.331(2)	Fe6−S7	2.416(2)
Fe6−Se2	2.329(2)	Fe1−Fe4′	4.507(2)
Fe1′-Fe4	4.190(2)	Fe1−Fe1′	6.187(3)
Fe4−Fe4′	6.111(3)		
Fe1−S7−Fe4	142.8(1)	Fe2−S7−Fe5	68.18(7)
Fe3−S7−Fe6	67.05(7)	Fe2−Se1−Fe5	71.28(6)
Fe3−Se2−Fe6	70.39(6)	Fe1−Se3−Fe4′	130.4(1)
Se3−Fe4′-S7′	122.4(1)	Se3−Fe1−S7	119.5(1)

[a] Mean value of intracubane distances.

$$2[(Tp)_2Mo_2Fe_6S_8(PEt_3)_4] + 6HSe^- \rightarrow [(Tp)_4Mo_4Fe_{12}S_{14.5}Se_{5.5}]^{5-} + 8PEt_3 + 3/2\ H_2 + H_2S + {}^1/_2\ HS^-/HSe^- \quad (6)$$

X-ray structure refinement indicates dominant occupancy of selenium atoms (≳90%) at the doubly bridging positions Se-(1,2,3) and full occupancy by sulfur atoms at other positions. For simplicity, in this figure, in Table 5 containing selected metric data, and below, the cluster is referred to as $[(Tp)_2Mo_2Fe_6S_7Se_3]_2^{5-}$, the composition if the foregoing three sites were occupied solely by selenium. We interpret the combined X-ray and analytical results in terms of the half-cluster formulation $Mo_2Fe_6(\mu_3\text{-}S)_6(\mu_6\text{-}S)(\mu_2\text{-}Se)_{2.75}(\mu_2\text{-}S)_{0.25}$; that is, the doubly bridging positions are occupied by ≲10% sulfur. The ^1H NMR spectrum of **9**, with two sets of pyrazolyl resonances in a 2:1 intensity ratio and similar chemical shifts (Figure 7), resembles the spectrum of **7**. Most of the signals are accompanied by very weak signals nearby (e.g., δ 8.04 near δ 7.80), which we attribute to species containing sulfide in one or more bridging positions.

The structure of cluster **9** features a central nonplanar eight-membered ring with four independent angles. The ring is bent along the Se(3,3′) vector with a dihedral angle of 147.5° between the plane Mo(1,2)Fe(1,4)S(7)Se(3,3′) and its symmetry-related counterpart. The two largest are Fe1−Se3−Fe4′ = 130.4(1)° and Fe1−S7−Fe4 = 142.8(1)°, the latter being nearly the same as Fe1−S8−Fe4 = 141.0(1)° in **7**. The remainder of the structure closely resembles **7**. The assigned positions of selenium atoms are consistent with observed bond lengths, as may be seen by the following comparisons of mean values for **9** vs **7**: Fe−(μ_2-Se) = 2.323(13) Å (mean of 6) vs Fe−(μ_2-S) = 2.225(5) Å (mean of 4); Fe−(μ_3-S) = 2.248(3) Å vs 2.263(7) Å (mean of 12); Fe−(μ_6-S) = 2.378(11) Å vs 2.359(2) Å (mean of 2),

(29) Bobrik, M. A.; Laskowski, E. J.; Johnson, R. W.; Gillum, W. O.; Berg, J. M.; Hodgson, K. O.; Holm, R. H. *Inorg. Chem.* **1978**, *17*, 1402−1410.
(30) Nelson, L. L.; Lo, F. Y. K.; Rae, A. D.; Dahl, L. F. *J. Organomet. Chem.* **1982**, *225*, 309−329.
(31) Greaney, M. A.; Coyle, C. L.; Pilato, R. S.; Stiefel, E. I. *Inorg. Chim. Acta* **1991**, *189*, 81−96.

2.428(11) Å vs 2.392(7) Å (mean of 4). The difference between Shannon radii for Se^{2-} and S^{2-} is 0.14 Å.[32]

A plausible conclusion from the selenide substitution results is that the source of the μ_6-S atom in **7** is a sulfide atom existent in the core precursor cluster **4** rather than external sulfide, which we take to be the intuitive source in reaction 4. A further intimation (and nothing more) is that the two μ_2-S atoms of **7** need not arise solely from core sulfide, a corollary being that the hydrosulfide ligands may not derive only from the added reagent. We also recognize that, through a complicated interplay of bond distances and angles (with selenium in general sustaining slightly smaller bridge angles), it may be energetically preferable to incorporate selenide rather than sulfide in doubly bridging positions, at least in a structure such as **9**. Here we treat selenium as a surrogate isotope of sulfur in order to decide the source—external or internal—of certain core sulfur atoms in **7**. Because this relationship between the elements is credible but not actual, we can only offer what are possible but not rigorously proven conclusions. The procedure by which the pathway of construction of cluster core **7** from **4** may be illuminated is not obvious.

Future reports will describe the vanadium analogue of cluster **7**, further reactions and properties of double cubane **4** and the P^N cluster analogue **7**, and experiments aimed at the FeMoco topology.

Acknowledgment. This research was supported by NIH Grant GM 28856. We thank Dr. J. Zuo for helpful discussion and Drs. H.-C. Zhou and P. V. Rao for experimental assistance.

Supporting Information Available: X-ray crystallographic files for the eight compounds in Tables 1 and 2. This material is available free of charge via the Internet at http://pubs.acs.org.

JA0214633

(32) Shannon, R. D. *Acta Crystallogr.* **1976**, *A32*, 751−767.